inorganics

MDPI

Article

Synthesis and Characterization of $NaCd_{0.92}Sn_{1.08}$, $Na(Cd_{0.28}Sn_{0.72})_2$ and Na_2CdSn_5 with Three-Dimensional Cd-Sn Frameworks

Yuki Asamiya [1,2], Takahiro Yamada [1,*] and Hisanori Yamane [1]

[1] Institute of Multidisciplinary Research for Advanced Materials, Tohoku University, Katahira, 2-1-1 Aoba-ku, Sendai 980-8577, Japan; yuki.asamiya.q8@dc.tohoku.ac.jp (Y.A.); hisanori.yamane.a1@tohoku.ac.jp (H.Y.)

[2] Department of Metallurgy, Materials Science and Materials Processing, Graduate School of Engineering, Tohoku University, 6-6-04 Aramaki Aza Aoba, Aoba-ku, Sendai 980-8579, Japan

* Correspondence: takahiro.yamada.b4@tohoku.ac.jp; Tel.: +81-22-217-5814

Abstract: The crystal structures of three new ternary compounds, $NaCd_{0.92}Sn_{1.08}$ (I), $Na(Cd_{0.28}Sn_{0.72})_2$ (II), and Na_2CdSn_5 (III) synthesized in a sodium-cadmium-tin system were determined by single-crystal X-ray analysis to be the following: (I) LiGeZn-type structure (hexagonal, a = 4.9326(1) Å, c = 10.8508(3) Å, space group P-6m2); (II) $CaIn_2$-type structure (hexagonal, a = 4.8458(2) Å, c = 7.7569(3) Å, $P6_3/mmc$); and (III) isotype with tI-Na_2ZnSn_5 (tetragonal, a = 6.4248(1) Å, c = 22.7993(5) Å, I-42d). Each compound has a three-dimensional framework structure mainly composed of four-fold coordinated Cd and Sn atoms with Na atoms located in the framework space. Elucidation of the electrical properties of the polycrystalline samples indicated that compounds (I) and (II) are polar intermetallics with metallic conductivity, and compound (III) is a semiconducting Zintl compound. These properties were consistent with the electronic structures calculated using the ordered structure models of the compounds.

Keywords: Zintl phases; polar intermetallics; crystal structures; electrical properties

Citation: Asamiya, Y.; Yamada, T.; Yamane, H. Synthesis and Characterization of $NaCd_{0.92}Sn_{1.08}$, $Na(Cd_{0.28}Sn_{0.72})_2$ and Na_2CdSn_5 with Three-Dimensional Cd-Sn Frameworks. *Inorganics* **2021**, *9*, 19. https://doi.org/10.3390/inorganics9030019

Academic Editor: Rainer Niewa

Received: 18 February 2021
Accepted: 4 March 2021
Published: 6 March 2021

1. Introduction

Intermetallic compounds composed of alkali or alkali earth metals (*A* and *AE*, respectively) and early p-block elements (groups 13–15; *B*) are classified as polar intermetallics and Zintl phases [1–4]. These intermetallic compounds are known to present a variety of crystal structures comprising various polyanions, such as clusters and networks formed by highly electronegative *B* atoms that receive electrons from the *A* and *AE* atoms with low electronegativity. These intermetallic compounds have ionic and covalent bonds and exhibit electrical properties ranging from metallic to semi-metallic, semiconducting, and even superconducting behaviors [5–8]. The potential applications of these intermetallic compounds for thermoelectric conversion, photovoltaic power generation, and catalytic reactions have been investigated [8–12]. Furthermore, first-principles calculations have predicted that many intermetallic compounds [13–16] are topological materials that display unique electronic properties. Therefore, the synthesis of new polar intermetallics and Zintl phases and the characterization of their crystal structures and electronic properties have attracted interest in recent years.

Recently, Fässler et al. studied ternary alkali metal compounds containing Sn (group 14 element) and Zn (group 12 late-transition metal element), and synthesized nine intermetallic compounds in the Na-Zn-Sn system [17–20]. The crystal structures of the synthesized compounds were determined by single-crystal X-ray diffraction (XRD), and their electrical properties were evaluated by density functional theory (DFT) calculations. Seven out of the nine compounds contain clusters of deltahedra or icosahedra composed of Sn and Zn atoms to which electrons are donated from the Na atoms. The icosahedral clusters are characteristic of the compounds of group 13 elements. While, two polymorphs (body-centered tetragonal lattice (*tI*) and hexagonal primitive lattice (*hP*) phases) have

been reported for a Sn-rich compound, Na_2ZnSn_5 [20]. Both phases have tetrahedrally coordinated Zn-Sn frameworks of which Na atoms are located in the tunnel spaces. Such tetrahedral coordination in the frameworks is observed in the pure substances of group 14 elements (Si, Ge, and α-Sn), and many Zintl clathrates such as Na_8Si_{46}, although various polyhedral clusters of group 14 elements are known in Zintl phases [3,4]. As *tI*-Na_2ZnSn_5 has semiconducting properties with a large Seebeck coefficient and low lattice thermal conductivity, it is expected to be a base material for thermoelectric materials [20,21].

Cd is a group 12 element like Zn, and three compounds—Na_2CdSn, $Na_{49}Cd_{58.5}Sn_{37.5}$, and $Na_{13}Cd_{20}Sn_7$ [22–24]—have been reported in the Na-Cd-Sn system. Na_2CdSn, which is rich in Na, has a Li_2CuAs-type structure (hexagonal a = 4.990 Å, c = 10.111 Å, space group $P6_3/mmc$). It includes a honeycomb sheet of Cd-Sn, similar to that of B-N in hexagonal boron nitride (BN), and Na atoms are situated between the sheets [22]. Recently, theoretical calculations predicted that Na_2CdSn has the electronic band structure of a typical Dirac semi-metal or topological insulator [15,25,26]. $Na_{49}Cd_{58.5}Sn_{37.5}$ (rhombohedral, a = 16.034(1) Å, c = 50.640(1) Å, R-3m) has a framework structure consisting of large closo-deltahedra and icosahedra of Cd/Sn atoms, in which Na atoms are located [23]. $Na_{13}Cd_{20}Sn_7$ (cubic, a = 15.790(4) Å, Im-3) features icosahedral Cd clusters and Cd/Sn polyhedra, and Na atoms are located in the polyhedra and at the gaps between the clusters [24]. Theoretical calculations and magnetic susceptibility measurements indicated that $Na_{49}Cd_{58.5}Sn_{37.5}$ and $Na_{13}Cd_{20}Sn_7$ have metallic band structures.

Sn-rich Na-Cd-Sn compounds, which could be expected to have three-dimensional frameworks composed of four-fold coordinated Cd and Sn atoms, as preferred in the structures of the group 14 atoms, have not been reported in previous studies. In the present study, an exploratory synthesis focusing on Sn-rich compositions was performed, and three new compounds, $NaCd_{0.92}Sn_{1.08}$, $Na(Cd_{0.28}Sn_{0.72})_2$, and Na_2CdSn_5, were synthesized. Herein, we report the syntheses, crystal structure, and electronic properties of these compounds.

2. Experimental

2.1. Synthesis of Na-Cd-Sn Compounds

Na (99.95 % purity, Nippon Soda Co. Ltd., Tokyo, Japan), Cd (99.9 % purity, Atom Shield Co. Ltd., Saitama, Japan), and Sn (99.999 % purity, Mitsuwa Chemicals Co. Ltd., Osaka, Japan) metals were used to synthesize the Na-Cd-Sn compounds. The Na metal was weighed in an Ar-filled glovebox (MBRAUN, Garching, Germany, O_2, H_2O < 1 ppm) to avoid reaction with oxygen and moisture in air, and the Cd and Sn metals were weighed in air at the prescribed molar ratios. The source metals (total mass of approximately 1.0 g) were put together in the Ar-filled glovebox and placed into a polycrystalline sintered BN crucible (purity, 99.5 %; inner diameter, 6.5 mm; depth, 18 mm; Showa Denko K.K., Tokyo, Japan) and sealed in a stainless steel (SUS 316) container (inner diameter of 10.7 mm, depth of 80 mm). The container was heated at 773 K for 2 h in an electric furnace to produce a melt-solidified bulk of the source metals. The obtained solid was pulverized using an agate mortar and pestle, and the powder was pressed into rectangular compacts ($14 \times 3 \times 3$ mm^3) by uniaxial die-pressing. The compacts were heated in a BN crucible in an Ar atmosphere at 593 K (for Na_2CdSn_5) and 673 K (for $NaCd_{0.92}Sn_{1.08}$ and $Na(Cd_{0.28}Sn_{0.72})_2$) for 36 h. The pulverizing-molding-heating process was repeated twice to prepare a polycrystalline sintered sample, which was used to identify the crystalline phases in the samples and evaluate the electrical properties. Single crystals used for crystal structure analysis were obtained by heating the source metals at 773 K for 2 h, and then cooling to 533 K at the rate of -4.0 Kh^{-1}.

2.2. Characterization

The polycrystalline sintered samples were pulverized and placed in a cell with a Mylar film window in an Ar atmosphere, and the powder XRD patterns were measured using a powder diffractometer (D2 PHASER, Bruker AXS, Karlsruhe, Germany) and Cu-Kα

radiation. Single crystals were sealed in a glass capillary under an Ar atmosphere, and the XRD data were collected using a single-crystal diffractometer (D8 QUEST, Bruker AXS Karlsruhe, Germany) with Mo Kα radiation. The APEX3 software package (version 2018.1-9, Bruker AXS, Madison, Wisconsin, USA) [27] was used to collect data, refine the lattice constants, and correct the X-ray absorption effect. The SHELXL-2018 program (version 2018/3) [28] and WinGX software (version 2018.3) [29] were used to analyze the crystal structures of the compounds. The VESTA software (version 3.5.3) [30] was used to visualize the crystal structures. COD 3000292, 3000293, and 3000294 contain the supplementary crystallographic data for this paper. These data can be obtained free of charge via http://www.crystallography.net/search.html (accessed on 8 February 2021).

Electrical resistivity (ρ) and Seebeck coefficient (S) of the sintered polycrystalline samples were measured by the direct current four-terminal and thermoelectric-power temperature-difference methods under an Ar atmosphere in the temperature range of 295–400 K. The electronic structures of the Na-Cd-Sn ternary compounds found in this study were calculated on the basis of the DFT calculations using the "*Advance/PHASE*" software package (Advance Soft Corp., Tokyo, Japan).

3. Results and Discussion

3.1. Synthesis of Polycrystalline Na-Cd-Sn Compounds

The polycrystalline bulk samples were synthesized from starting materials with Na:Cd:Sn molar ratios of approximately 1:1:1, 2:1:3, and 2:1:5 (Na:Cd:Sn = 1:(1−s):(1 + s), s = 0, 0.05, 0.06, 0.08, 0.09, 0.100; Na:Cd:Sn = 1:2t:2(1−t), t = 0.25, 0.275, 0.28, 0.29, 0.30; and Na:Cd:Sn = (2 + u):(1 + u/2):(5−u/2), u = −0.05, 0.0, 0.05). The maximum difference in mass before and after melting the raw materials at 733–773 K was approximately ±1.5 mg against 1 g of the total initial amount of raw materials. If this change was attributed to the evaporation of Na or Cd, both of which have relatively high vapor pressures, then the maximum change of the sample compositions was estimated to be 1.5 at% for Na and 0.5 at% for Cd. The change in mass after heating at 593–673 K in the pulverizing-molding-heating process was within the weighing error. Thus, the initial starting compositions were regarded as the sample compositions obtained in the present study.

XRD patterns that could not be identified for any of the reported Na-Cd-Sn compounds were observed in the obtained samples. As shown in Figure 1, the unidentified XRD patterns resemble those of LiZnGe (hexagonal a = 4.2775(3) Å, c = 9.3653(8) Å, space group P-6m2) [31], Li_2ZnGe_3 ($Li(Zn_{0.25}Ge_{0.75})_2$, hexagonal a = 4.167 (1) Å, c = 6.754(1) Å, $P6_3mmc$) [32], and tI-Na_2ZnSn_5 (tetragonal, a = 6.3410(5) Å, c = 22.3947(18) Å I-42d) [20]. These compounds consisted of groups 1, 12, and 14. The XRD patterns of the samples with Na:Cd:Sn ratios of 1:0.92:1.08 (s = 0.08), 1:0.56:1.44 (t = 0.28), and 2:1:5 (u = 0.0) were closest to the single-phase patterns, although trace peaks of Cd and/or Sn were observed (Figure 1). Cd and Sn were probably formed by degradation during sample handling and XRD measurements because the new compounds were unstable in the presence of moisture in air. Therefore, the compositions of the new phases were determined to be $NaCd_{0.92}Sn_{1.08}$, $Na_2Cd_{1.12}Sn_{2.88}$, and Na_2CdSn_5. The lattice constants of the new Na-Cd-Sn compounds refined by powder XRD were as follows: $NaCd_{0.92}Sn_{1.08}$, hexagonal, a = 4.9348(3) Å and c = 10.8573(8) Å; $Na_2Cd_{1.12}Sn_{2.88}$ [= $Na(Cd_{0.28}Sn_{0.72})_2$], hexagonal, a = 4.8474(2) Å and c = 7.7609(3) Å; and tI-Na_2CdSn_5, tetragonal, a = 6.4255(2) Å and c = 22.8007(8) Å.

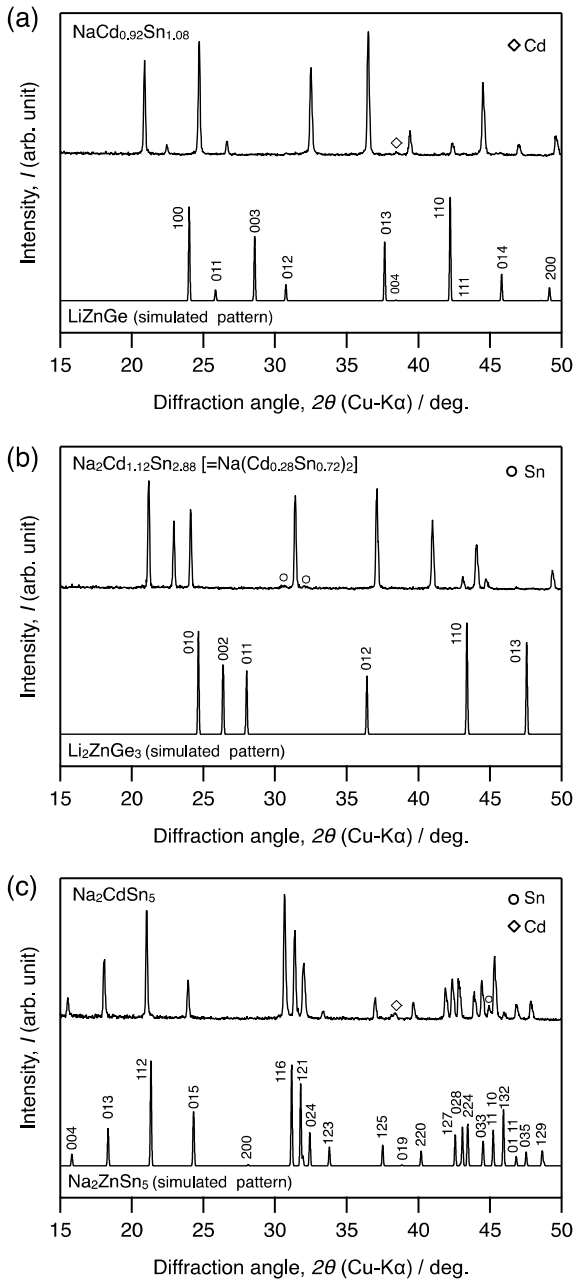

Figure 1. Powder XRD patterns of the polycrystalline samples prepared from starting materials with molar ratios of Na:Cd:Sn = 1:0.92:1.08 (**a**), 2:1.12:2.88 (**b**), and 2:1:5 (**c**) (upper patterns), and the simulated XRD patterns of isostructural compounds, LiZnGe (**a**), Li_2ZnGe_3 (**b**), and *tI*-Na_2ZnSn_5 (**c**) (lower patterns).

3.2. Crystal Structure

The crystallographic and refinement details of the single-crystal XRD structure analysis for $NaCd_{0.92}Sn_{1.08}$, $Na(Cd_{0.28}Sn_{0.72})_2$, and *tI*-Na_2CdSn_5 are presented in Table 1. The atomic coordinates, equivalent isotropic atomic displacement parameters (ADPs), and interatomic distances are summarized in Tables 2 and 3, and the anisotropic ADPs are listed in Table S1.

Table 1. Crystallographic data for $NaCd_{0.92}Sn_{1.08}$, $Na(Cd_{0.28}Sn_{0.72})_2$, and *tI*-Na_2CdSn_5.

Chemical Formula	$NaCd_{0.92}Sn_{1.08}$	$Na(Cd_{0.28}Sn_{0.72})_2$	Na_2CdSn_5
Crystal Form	block	block	block
Crystal Size/μm^3	28 × 86 × 134	32 × 65 × 92	93 × 125 × 197
Formula Weight, M_r /g mol^{-1}	254.58	256.85	751.83
Crystal System	hexagonal	hexagonal	tetragonal
Space Group, *Z*	$P\bar{6}m2$, 3	$P6_3/mmc$, 2	$I\bar{4}2d$, 4
Radiation, λ/Å	0.71073	0.71073	0.71073
F_{000}	327	220	1280
Temperature, *T*/K	300(2)	298(2)	299(2)
Unit Cell Dimensions			
a/Å	4.93260(10)	4.8458(2)	6.42700(10)
c/Å	10.8508(3)	7.7569(3)	22.8086(5)
Unit Cell Volume, *V*/Å^3	228.636(11)	157.743(14)	942.14(4)
Calculated Density, D_{cal}/Mgm^{-3}	5.547	5.408	5.300
Absorption Coefficient, μ/m^{-1}	15.064	14.980	15.268
Limiting Indices			
h	$-6 \le h \le 6$	$-6 \le h \le 8$	$-11 \le h \le 10$
k	$-6 \le k \le 6$	$-7 \le k \le 8$	$-10 \le k \le 11$
l	$-14 \le l \le 14$	$-12 \le l \le 8$	$-41 \le l \le 41$
θ Range for Data Collection	3.756–28.261	4.858–36.227	3.293–40.228
Reflections Collected/Unique	3258/271	1617/170	11489/1481
R_{int}	0.0322	0.0266	0.0328
Data/Restrains/Parameters	271/0/18	170/0/7	1481/0/24
Extinction Coefficient, *x*	0.011(2)	0.0118(17)	0.0056(2)
Flack parameter	0.08(8)	–	0.04(7)
Goodness-of-Fit on F^2, *S*	1.160	1.234	1.277
*R*1, *wR*2 ($I > 2\sigma$ (*I*))	0.0178, 0.0408	0.0143, 0.0270	0.0197, 0.0325
*R*1, *wR*2 (all data)	0.0178, 0.0408	0.0164, 0.0276	0.0228, 0.0334
Largest Diffraction Peak and Hole, $\Delta\rho$/e Å^{-3}	1.023, −1.554	1.353, −0.648	1.065, −0.969

Table 2. Atomic coordinates and equivalent isotropic displacement parameters of $NaCd_{0.92}Sn_{1.08}$, $Na(Cd_{0.28}Sn_{0.72})_2$, and *tI*-Na_2CdSn_5.

Atom	Site	Occ.	*x*	*y*	*z*	U_{eq}(Å)
$NaCd_{0.92}Sn_{1.08}$						
Na1	1*d*	1	1/3	2/3	1/2	0.0242(18)
Na2	2*h*	1	1/3	2/3	0.1654(6)	0.0242(12)
Cd/Sn1	1*e*	0.92/0.08	2/3	1/3	0	0.0265(4)
Cd/Sn2	2*g*	0.92/0.08	0	0	0.29945(15)	0.0236(3)
Sn1	1*a*	1	0	0	0	0.0147(3)
Sn2	2*i*	1	2/3	1/3	0.36068(8)	0.0122(3)
$Na(Cd_{0.28}Sn_{0.72})_2$						
Na1	2*b*	1	1	0	1/4	0.0273(6)
Cd/Sn1	4*f*	0.28/0.72	1/3	2/3	0.05416(3)	0.01576(10)
***tI*-Na_2CdSn_5**						
Na1	16*e*	1/2	0.1517(7)	0.2132(13)	0.1398(3)	0.064(3)
Cd1	4*a*	1	0	0	0	0.01813(8)
Sn1	16*e*	1	0.16221(3)	0.15809(3)	0.31679(2)	0.01457(5)
Sn2	4*b*	1	0	0	1/2	0.01345(7)

Table 3. Selected interatomic distances within 4 Å for $NaCd_{0.92}Sn_{1.08}$, $Na(Cd_{0.28}Sn_{0.72})_2$, and *tI*-Na_2CdSn_5.

Compounds and Atomic Sites		Distance (Å)
$NaCd_{0.92}Sn_{1.08}$		
Sn1	-Cd/Sn1	2.84784(6)
Sn1	-Cd/Sn2	3.2492(17)
Sn2	-Sn2	3.0235(18)
Sn2	-Cd/Sn2	2.9243(5)
Sn1	-Na2	3.366(4)
Sn2	-Na1	3.2242(5)
Sn2	-Na2	3.550(4)
Cd/Sn1	-Na2	3.366(4)
Cd/Sn2	-Na2	3.198(4)
$Na(Cd_{0.28}Sn_{0.72})_2$		
Cd/Sn1	-Cd/Sn1	2.92115(19), 3.0382(5)
Cd/Sn1	-Na1	3.18354(17), 3.6598(2)
***tI*-Na_2CdSn_5**		
Sn1	-Sn1	2.8854(4), 2.9115(4)
Sn1	-Sn2	2.8400(2)
Cd1	-Sn1	2.8699(2)
Na1	-Na1	0.824(14), 3.363(16), 3.819(5)
Na1	-Sn1	3.176(8), 3.287(9), 3.419(5), 3.495(5), 3.598(5), 3.670(5)
Na1	-Cd1	3.266(8), 3.604(8)
Na1	-Sn2	3.634(6)

3.2.1. $NaCd_{0.92}Sn_{1.08}$

The crystal structure of $NaCd_{0.92}Sn_{1.08}$ was initially refined using a structural model of LiZnGe. Li (1*d* and 2*h* sites), Zn (1*e*, 2*g*), and Ge (1*a*, 2*i*) were replaced with Na, Cd, and Sn, respectively. The reliability factors, *R*1 and *wR*2, of the refinement for all data were 1.78 and 4.20%, respectively. In general, it is difficult to distinguish between atoms with similar X-ray scattering powers, such as Cd and Sn, by XRD. Indeed, the occupancies of Cd and Sn atoms could not be refined by placing both Cd and Sn atoms at the Zn(1*e*, 2*g*) and Ge (1*a*, 2*i*) sites. The other three ordered configurations of Cd and Sn atoms and Cd/Sn equimolar occupation at the four sites of Zn (1*e*, 2*g*) and Ge (1*a*, 2*i*) resulted in *R*1 values of 2.06–2.96% larger than that of the initial model (1.78%) (Table S2). When 8% of the Cd atoms were replaced with Sn at the 1*e* and 2*g* sites in accordance with the composition of the polycrystalline sample ($NaCd_{0.92}Sn_{1.08}$), the *R*1 value was the same (1.78%), but *wR*2 decreased slightly from 4.20% to 4.08%. Thus, the final refinement was performed with a composition of $NaCd_{0.92}Sn_{1.08}$.

The crystal structure of $NaCd_{0.92}Sn_{1.08}$ (hexagonal, a = 4.9326(1) Å, c = 10.8508(3) Å, *P*-6*m*2) is shown in Figure 2. Cd and Sn atoms form a three-dimensional framework, and Na atoms are arranged in the channels. The interatomic distances between Na and Cd or Na and Sn ranged between 3.198(3) Å and 3.550(4) Å, whereas the distances between the Cd and Sn atoms were between 2.84784(6) Å and 3.2492(17) Å (see Table 3 and Figure 2b,c). The Cd-Sn framework comprises a flat honeycomb sheet of Cd/Sn1 and Sn1 (A) and two puckered honeycomb layers of Cd/Sn2 and Sn2 (B and B'). The sheet and layers are stacked in the sequence ABB' in the *c*-axis direction. Focusing on the Cd/Sn2-centered distorted tetrahedra of Sn1 and Sn2, the tetrahedra form double layers on the *ab* plane, sandwiching the Cd/Sn1-Sn1 honeycomb sheet by sharing the vertex Sn1 atoms. The interatomic distance between the Cd/Sn1 and Sn1 atoms in the flat honeycomb sheet was 2.84784(6) Å. The distances between the central Cd/Sn2 and vertex Sn atoms of the tetrahedra were 3.2492(17) Å ($d_{Cd/Sn2\text{-}Sn1}$) and 2.9243(5) Å ($d_{Cd/Sn2\text{-}Sn2}$), and the distance between the Sn2 atoms in the tetrahedral layer was 3.0235(18) Å.

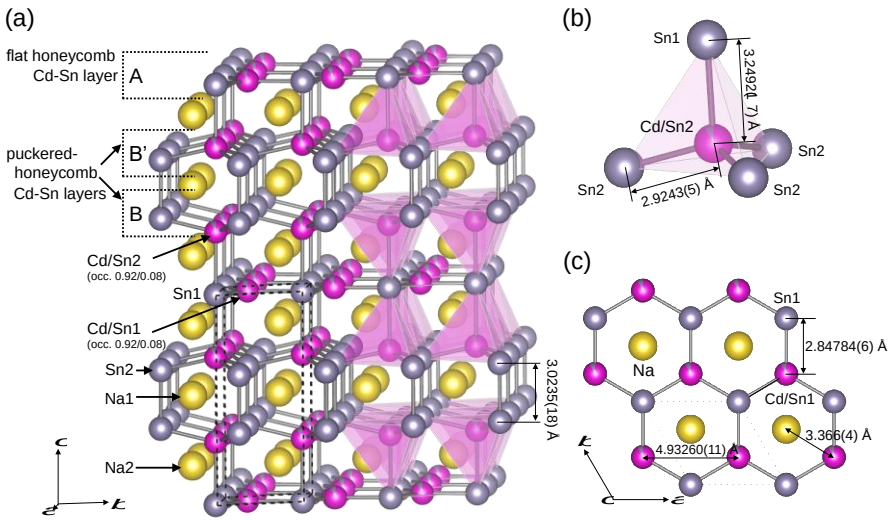

Figure 2. Crystal structure of $NaCd_{0.92}Sn_{1.08}$: a general view (**a**), a structural motif of Cd/Sn2-centered Sn tetrahedron, and (**b**) Cd-Sn honeycomb sheet (**c**).

The previously reported Na-Cd-Sn compound, Na_2CdSn, (hexagonal, $P6_3mmc$, a = 4.990 Å, and c = 10.111 Å) [22] has a Li_2CuAs-type crystal structure in which a Na atom layer and a flat Cd-Sn honeycomb lattice sheet similar to that of the $NaCd_{0.92}Sn_{1.08}$ stack alternately. The interatomic distance between the Cd and Sn atoms of the honeycomb sheet in Na_2CdSn is 2.881 Å, which is comparable to that in $NaCd_{0.92}Sn_{1.08}$ (2.84784(6) Å).

3.2.2. $Na(Cd_{0.28}Sn_{0.72})_2$

The crystal structure of $Na(Cd_{0.28}Sn_{0.72})_2$ was derived to be of $CaIn_2$-type with hexagonal lattice parameters of a = 4.8458(2) Å, c = 7.7569(3) Å, and space group $P6_3/mmc$ (No. 194). The refinement gave the $R1$ and $wR2$ values of 1.64 and 2.76%, respectively, for all data (Table 1). The structure of $Na(Cd_{0.28}Sn_{0.72})_2$ consists of two crystallographically independent atomic positions: the Na1 (12*d*) and Cd/Sn1 (6*d*) sites. The occupancies of Cd and Sn in the Cd/Sn1 site were fixed to be 0.28/0.72 in accordance with the source composition from which the single-phase sample was obtained. As illustrated in Figure 3, the atoms at the Cd/Sn1 site are tetrahedrally coordinated with each other and form a three-dimensional framework. The arrangement of the Cd/Sn1 atoms is similar to that of the C atoms in lonsdaleite (hexagonal diamond). The layer of puckered Cd/Sn six-membered rings in the *ab* plane were stacked in an AB order in the direction of the *c*-axis. The Cd/Sn interatomic distance in the *c*-axis direction (3.0382(5) Å) was longer than the interatomic distance between the other three equivalent Cd/Sn atoms (2.92117(18) Å). Na atoms are located between the Cd/Sn layers and surrounded by 12 Cd/Sn1 atoms with Na-Cd/Sn distances of 3.18354(16) and 3.65795(19) Å. Several $CaIn_2$-type intermetallic compounds have been reported in the *A*-*M*-*Tt* systems (*A*: alkali metal, *M*: group 12 element, *Tt*: tetrelide). Li_2ZnGe_3 [$Li(Zn_{0.25}Ge_{0.75})_2$; hexagonal a = 4.167(1) Å and c = 6.754(1) Å] has a Zn/Ge ratio of 0.25/0.75 [32], which is close to the Cd/Sn ratio of 0.28/0.72 in $Na(Cd_{0.28}Sn_{0.72})_2$.

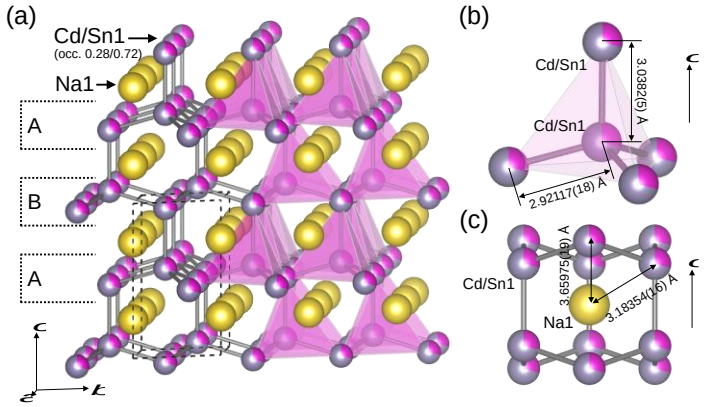

Figure 3. Crystal structure of $Na(Cd_{0.28}Sn_{0.72})_2$: a general view (**a**), a Cd/Sn1 tetrahedron (**b**), and an arrangement of Cd/Sn1 around Na1 (**c**).

3.2.3. Na_2CdSn_5

Na_2CdSn_5 crystallizes in a tetragonal cell with the lattice parameters of a = 6.42700(10) Å and c = 22.8086(5) Å, space group I-42d. It is isostructural with t*I*-Na_2ZnSn_5 (tetragonal, a = 6.3410(5) Å, c = 22.3947(18) Å, I-42d) [21], which is one of the two polymorphs of Na_2ZnSn_5 [20]. When the crystal structure of t*I*-Na_2ZnSn_5 was used as a starting model for the refinement, the reliability factors R1 and wR2 were 2.28 and 3.34%, respectively, for all data (Table 1). In this model, Cd and Sn atoms are arranged in an orderly manner, as shown in Figure 4. A refinement using a model in which Cd and Sn atoms are statistically located at the atomic sites of the framework with an occupancy of 1/6 Cd and 5/6 Sn gave R1 and wR2 values of 2.48% and 4.49%, respectively, which are larger than those of the ordered model.

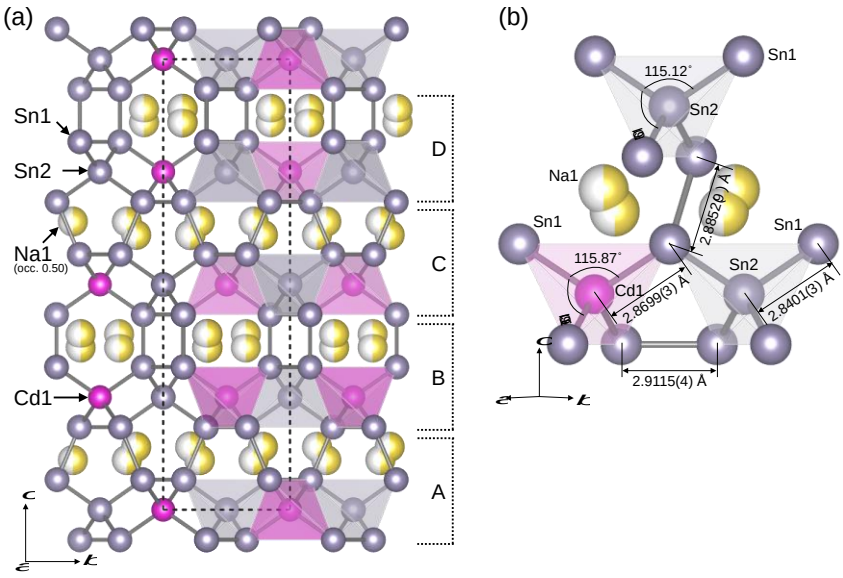

Figure 4. Crystal structure of Na_2CdSn_5: a projection on the b-c plane (**a**) and an arrangement of Cd-Sn tetrahedra (**b**).

The atomic sites of Na_2CdSn_5 are Cd1 (4a), Sn1 (16e), Sn2 (4b), and Na1 (16e). The atoms at the Cd1, Sn1, and Sn2 sites are tetrahedrally coordinated with each other and form a three-dimensional framework, in which spiral tunnel-like spaces extend in the a- and b-axis directions. The Na atoms are statistically situated at the split site of Na1 (16e) with an occupancy of 0.5 in the spaces. The layers of the unit, which are composed of Cd1- and Sn2-centered $Sn1_4$ tetrahedra (Cd1-$Sn1_4$ and Sn2-$Sn1_4$) and Na1 on the ab plane, stack in an ABCD sequence in the c-axis direction (Figure 4). The Cd-Sn distances of

the Cd1-centered and Sn2-centered Sn1 tetrahedra are 2.8699(3) × 4 and 2.8401(3) Å × 4, respectively, and the Sn1-Sn1 distances between the Cd1- and Sn2-centered Sn1 tetrahedra are 2.9115(4) Å in the *ab* plane and 2.8852(9) Å in the *c*-axis direction. The lattice volume (942.14 Å^3) of Na_2CdSn_5 is 4.6% greater than that of *tI*-Na_2ZnSn_5 (900.45 Å^3) [21]. The Cd-Sn distance in the Cd1-$Sn1_4$ tetrahedra is 4.3 % larger than the Zn-Sn distance (2.7509 Å) of the Zn1-$Sn1_4$ tetrahedra of the *tI*-Na_2ZnSn_5 (Table S3). These differences are consistent with the difference between the covalent radii of Cd (1.40 Å) and Zn (1.20 Å) [33].

The equivalent isotropic atomic displacement parameter (U_{eq}) of Na1 in Na_2CdSn_5 is 0.064 Å^2, which is approximately four times larger than the U_{eq} of Cd1, Sn1, and Sn2 (0.01345–0.01812 Å^2), and approximately three times larger than that of the Na atoms of $NaCd_{0.92}Sn_{1.08}$ and $Na(Cd_{0.28}Sn_{0.72})_2$ (0.0242–0.0273 Å^2). Similar large U_{eq} values of Na have also been reported for *tI*-Na_2ZnSn_5 (0.055 Å^2), *hP*-Na_2ZnSn (0.080 Å^2) [21], $Na_{2.19}Ga_{2.19}Sn_{3.18}$ (0.084 Å^2) [34], and $Na_{1.76}Al_{1.76}Sn_{4.24}$ (0.080 Å^2) [35], which have spiral tunnel frameworks. The Na ADPs of these compounds significantly decreased with decreasing temperature, indicating that the Na atoms exhibit large thermal vibration. This contributes to the reduction in the thermal conductivity of the lattice, leading to enhanced thermoelectric properties of the compounds [21,34,35].

3.3. Electrical Properties

The electrical resistivity (ρ) of the polycrystalline samples of $NaCd_{0.92}Sn_{1.08}$, $Na(Cd_{0.28}Sn_{0.72})_2$, and Na_2CdSn_5 in the temperature range of 295–400 K are shown in Figure 5. The relative densities of the samples were 87, 74, and 74 % of the theoretical densities of $NaCd_{0.92}Sn_{1.08}$, $Na(Cd_{0.28}Sn_{0.72})_2$, and Na_2CdSn_5, respectively. The ρ values of the $NaCd_{0.92}Sn_{1.08}$ and $Na(Cd_{0.28}Sn_{0.72})_2$ samples at 300 K were 0.14 and 1.21 mΩ cm, respectively. The values increased slightly with increasing temperature and reached 0.17 mΩ cm ($NaCd_{0.92}Sn_{1.08}$, 399 K) and 1.28 mΩ cm ($Na(Cd_{0.28}Sn_{0.72})_2$, 401 K) at the highest measurement temperatures. Whereas, the ρ value for the sample of Na_2CdSn_5 at 300 K was 1.36 Ω cm, which was three to four orders of magnitude larger than those of the $NaCd_{0.92}Sn_{1.08}$ and $Na(Cd_{0.28}Sn_{0.72})_2$ samples. The ρ value of the Na_2CdSn_5 sample decreased significantly with increasing temperature and reached a value of 0.30 Ω cm at 395 K. The Seebeck coefficients (S) of $NaCd_{0.92}Sn_{1.08}$ and $Na(Cd_{0.28}Sn_{0.72})_2$ were small positive values of +5.7 and +9.0 μV K^{-1}, respectively, at 300 K, while the S value of Na_2CdSn_5 had a large positive value of +568 μV K^{-1}. The S values and temperature dependences of ρ measured for the sintered samples indicate that the electronic structures of $NaCd_{0.92}Sn_{1.08}$ and $Na(Cd_{0.28}Sn_{0.72})_2$ are metallic, while that of Na_2CdSn_5 is semiconducting.

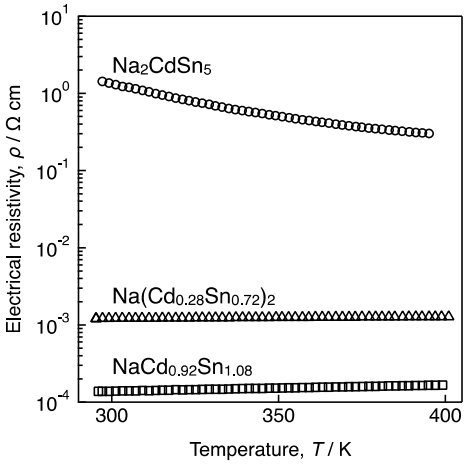

Figure 5. Electrical resistivities of the polycrystalline samples of $NaCd_{0.92}Sn_{1.08}$ (open squares), $Na(Cd_{0.28}Sn_{0.72})_2$ (open triangles), and Na_2CdSn_5 (open circles).

To elucidate the electrical properties of the compounds found in this study, the electronic band structures were examined. As $NaCd_{0.92}Sn_{1.08}$ and $Na(Cd_{0.28}Sn_{0.72})_2$ have mixed Cd/Sn sites, and the Na atoms in Na_2CdSn_5 statistically occupy the Na1 site with an occupancy of 0.5 in their crystal structures, the total and partial electronic densities of states (DOS) (Figure 6) were calculated using the ordered models of NaCdSn, $Na(Cd_{1/4}Sn_{3/4})_2$, and Na_2CdSn_5 shown in Figure S1. For NaCdSn and $Na(Cd_{1/4}Sn_{3/4})_2$, the electronic states near the Fermi level have a finite DOS, and there is a deep dip at approximately 0.4–0.6 eV above the Fermi level. Na_2CdSn_5 presented a band gap of approximately 0.3 eV and the DOSs at the top of the valence band and the bottom of the conduction band are both large, leading to a large *S* value. The results of this calculation provide a good description of the metallic behavior in terms of ρ and the low *S* values of $NaCd_{0.92}Sn_{1.08}$ and $Na(Cd_{0.28}Sn_{0.72})_2$ and the semiconducting behavior in terms of ρ and the large *S* value of Na_2CdSn_5. The activation energy calculated from the Arrhenius plot of the electrical conductivity of the Na_2CdSn_5 sample is approximately 0.15 eV, which is consistent with the band gap of 0.3 eV presented by the DOS calculation.

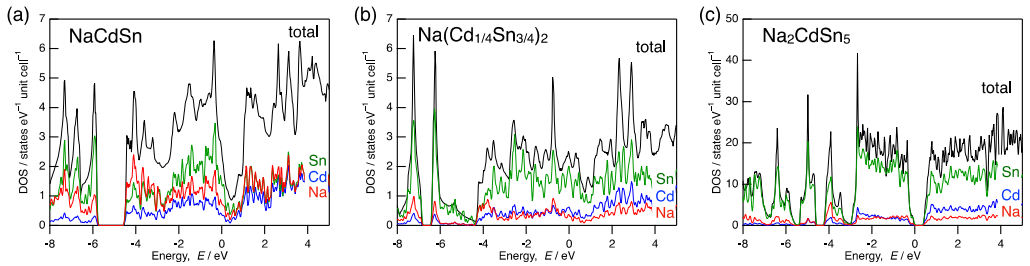

Figure 6. Total and partial DOSs calculated with ordered structure models for NaCdSn (**a**), $Na(Cd_{1/4}Sn_{3/4})_2$ (**b**), and Na_2CdSn_5 (**c**).

It has been reported that a polycrystalline bulk sample of *tI*-Na_2ZnSn_5 (relative density: 94%), which is isostructural with Na_2CdSn_5, exhibited semiconducting properties, and the ρ and *S* values at 295 K were 362 Ω cm and −455 μV K^{-1}, respectively. The lattice thermal conductivity of *tI*-Na_2ZnSn_5 was estimated to be 0.61 W m^{-1} K^{-1}, which may be caused by the large thermal vibration (rattling) of the Na atoms [21]. The ρ and *S* values measured for the Na_2CdSn_5 sample with a relative density of 74% are similar to those obtained for *tI*-Na_2ZnSn_5, although the sign of the Seebeck coefficient is different. Moreover, the distribution of the calculated DOS near the Fermi level is similar [20]. Therefore, Na_2CdSn_5 could be employed as a thermoelectric material by adjusting the carrier density with an appropriate amount of dopant.

4. Conclusions

Three new Na-Cd-Sn compounds, $NaCd_{0.92}Sn_{1.08}$, $Na(Cd_{0.28}Sn_{0.72})_2$, and Na_2CdSn_5, were synthesized, and their crystal structures were determined by single-crystal XRD. These compounds have three-dimensional frameworks formed by the Cd and Sn atoms, in which the Na atoms are incorporated. In the structure of $NaCd_{0.92}Sn_{1.08}$, four-coordinated tetrahedra of Cd and Sn atoms sandwich a Cd-Sn honeycomb sheet and Na atom layers. The structure of $Na(Cd_{0.28}Sn_{0.72})_2$ was characterized as a framework comprising four-coordinated Cd and Sn atoms similar to the arrangement of C atoms in lonsdaleite; Na atoms were included in the voids of the framework. These compounds are polar intermetallics with metallic properties. Na_2CdSn_5 is a typical Zintl compound described by the formulation $[Na^+]_2[Cd^{2-}][Sn^0]_5$. It is a semiconductor with a small band gap and has a framework structure composed of Cd and Sn-centered Sn_4 tetrahedra. Na atoms with large ADPs are situated in the tunnel-like spaces within the framework.

Supplementary Materials: The following are available online at https://www.mdpi.com/2304-6740/9/3/19/s1, Figure S1: Ordered structure models for DFT calculations, Table S1: Anisotropic

displacement parameters of three Na-Cd-Sn compounds found in this study, Table S2: Structure refinement results of NaCdSn based on the crystal structure of LiZnGe, Table S3: Selected interatomic distances for Na_2CdSn_5 and *tI*-Na_2ZnSn_5, A combined CIF and checkCIF for all discussed crystal structures.

Author Contributions: Y.A. and T.Y. conducted the sample preparation and phase identification, while the crystal structure analysis was performed by T.Y. and H.Y.; T.Y. accomplished the electronic structure calculation, independently designed and supervised the project. The manuscript was written with input from all authors (Y.A., T.Y., and H.Y.), who approved the final version of the manuscript. All authors have read and agreed to the published version of the manuscript.

Funding: This research was financially supported by JSPS KAKENHI Grant (JP20H02820).

Acknowledgments: The authors would like to thank Chikako Nagahama (Tohoku University) for helping with sample preparation.

Conflicts of Interest: The authors declare no conflict of interest.

References

1. Schäfer, H.; Eisenman, B.; Müller, W. Zintl Phases: Transitions between Metallic and Ionic Bonding. *Angew. Chem. Int. Ed.* **1973**, *12*, 694–712. [CrossRef]
2. Corbett, J.D. Exploratory Synthesis: The Fascinating and Diverse Chemistry of Polar Intermetallic Phases. *Inorg. Chem.* **2010**, *49*, 13–28. [CrossRef]
3. Shevelkov, A.V.; Kovnir, K. *Structure and Bonding 139 Zintl Phases: Principles and Recent Developments*; Fässler, T.F., Mingos, D.M.P., Eds.; Springer: Berlin/Heidelberg, Germany, 2011; Volume 139, pp. 97–142.
4. Fässler, T.F. *Structure and Bonding 140 Zintl Ions: Principles and Recent Developments*; Fässler, T.F., Mingos, D.M.P., Eds.; Springer: Berlin/Heidelberg, Germany, 2011; Volume 140, pp. 91–131.
5. Kusakabe, K.; Geshi, M.; Tsukamoto, H.; Suzuki, N. New half-metallic materials with an alkaline earth element. *J. Phys. Condens. Matter* **2004**, *16*, S5639–S5644. [CrossRef]
6. Fortner, J.; Saboungi, M.-L.; Enderby, J.E. Carrier Density Enhancement in Semiconducting NaSn and CsPb. *Phys. Rev. Lett.* **1995**, *74*, 1415–1418. [CrossRef] [PubMed]
7. Nagamatsu, J.; Nakagawa, N.; Muranaka, T.; Zenitani, Y.; Akimitsu, J. Superconductivity at 39 K in magnesium diboride. *Nature* **2001**, *410*, 63–64. [CrossRef]
8. Fässler, T.F.; Kronseder, C. $BaSn_3$: A Superconductor at the Border of Zintl Phases and Intermetallic Compounds. Real-Space Analysis of Band Structures. *Angew. Chem. Int. Ed.* **1997**, *36*, 2683–2686.
9. Suemasu, T.; Usami, N. Exploring the potential of semiconducting $BaSi_2$ for thin-film solar cell applications. *J. Phys. D Appl. Phys.* **2016**, *50*, 023001. [CrossRef]
10. Kauzlarich, S.M.; Zevalkink, A.; Toberer, E.; Snyder, G.J. Chapter 1 Zintl Phases: Recent Developments in Thermoelectrics and Future Outlook. In *Thermoelectric Materials and Devices*; Royal Society of Chemistry (RSC): London, UK, 2016; pp. 1–26.
11. Kauzlarich, S.M.; Brown, S.R.; Snyder, G.J. Zintl phases for thermoelectric devices. *Dalton Trans.* **2007**, 2099–2107. [CrossRef] [PubMed]
12. Hodge, K.L.; Goldberger, J.E. Transition Metal-Free Alkyne Hydrogenation Catalysis with $BaGa_2$, a Hydrogen Absorbing Layered Zintl Phase. *J. Am. Chem. Soc.* **2019**, *141*, 19969–19972. [CrossRef] [PubMed]
13. Yamada, T.; Deringer, V.L.; Dronskowski, R.; Yamane, H. Synthesis, Crystal Structure, Chemical Bonding, and Physical Properties of the Ternary Na/Mg Stannide Na_2MgSn. *Inorg. Chem.* **2012**, *51*, 4810–4816. [CrossRef]
14. Yamada, T.; Ikeda, T.; Stoffel, R.P.; Deringer, V.L.; Dronskowski, R.; Yamane, H. Synthesis, Crystal Structure, and High-Temperature Phase Transition of the Novel Plumbide Na_2MgPb. *Inorg. Chem.* **2014**, *53*, 5253–5259. [CrossRef] [PubMed]
15. Peng, B.; Yue, C.; Zhang, H.; Fang, Z.; Weng, H. Predicting Dirac semimetals based on sodium ternary compounds. *Npj Comput. Mater.* **2018**, *4*, 68. [CrossRef]
16. Wang, C.; Chen, Y.B.; Yao, S.-H.; Zhou, J. Low lattice thermal conductivity and high thermoelectric figure of merit in Na_2MgSn. *Phys. Rev. B* **2019**, *99*, 024310. [CrossRef]
17. Kim, S.J.; Hoffman, S.D.; Fässler, T.F. $Na_{29}Zn_{24}Sn_{32}$: A Zintl phase containing a novel type of $\{Sn_{14}\}$ enneahedra and heteroatomic $\{Zn_8Sn_4\}$ icosahedra. *Angew. Chem. Int. Ed.* **2007**, *46*, 3144–3148. [CrossRef]
18. Kim, S.J.; Kraus, F.; Fässler, T.F. Na_6ZnSn_2, $Na_{4.24}K_{1.76(1)}ZnSn_2$, and $Na_{20}Zn_8Sn_{11}$: Three Intermetallic Structures Containing the Linear $\{Sn\text{-}Zn\text{-}Sn\}^{6-}$ Unit. *J. Am. Chem. Soc.* **2009**, *131*, 1469–1478. [CrossRef]
19. Ponou, S.; Kim, S.J.; Fässler, T.F. Synthesis and Characterization of $Na_5M_{2+x}Sn_{10-x}$ (x approximate to 0.5, M = Zn, Hg)-A Doped Tetrahedral Framework Structure. *J. Am. Chem. Soc.* **2009**, *131*, 10246–10252. [CrossRef] [PubMed]
20. Stegmaier, S.; Kim, S.J.; Henze, A.; Fässler, T.F. Tetrahedral Framework Structures: Polymorphic Phase Transition with Reorientation of Hexagonal Helical Channels in the Zintl Compound Na_2ZnSn_5 and Its Relation to $Na_5Zn_{2+x}Sn_{10-x}$. *J. Am. Chem. Soc.* **2013**, *135*, 10654–10663. [CrossRef]

21. Kanno, M.; Yamada, T.; Ikeda, T.; Nagai, H.; Yamane, H. Thermoelectric Properties of Na_2ZnSn_5Dimorphs with Na Atoms Disordered in Tunnels. *Chem. Mater.* **2017**, *29*, 859–866. [CrossRef]
22. Matthes, R.; Schuster, H.-U. Ternäre Natriumphasen mit Cadmium bzw. Quecksilber und Zinn bzw. Blei/Ternary Sodium Phases with Cadmium or Mercury and Tin or Lead. *Z. Nat. B* **1980**, *35*, 778–780. [CrossRef]
23. Todorov, E.; Sevov, S.C. Synthesis, characterization, electronic structure, and bonding of heteroatomic deltahedral clusters: $Na_{49}Cd_{58.5}Sn_{37.5}$, a network structure containing the first empty icosahedron without a group 13 element and the largest closo-deltahedron. *J. Am. Chem. Soc.* **1997**, *119*, 2869–2876. [CrossRef]
24. Todorov, E.; Sevov, S.C. Synthesis, characterization, and bonding of heteroatomic clusters: $Na_{13}Cd_{20}E_7$ (E = Pb, Sn), a further example of a structure containing empty icosahedra without an element of group 13. *Inorg. Chem.* **1997**, *36*, 4298–4302. [CrossRef]
25. Tang, F.; Po, H.C.; Vishwanath, A.; Wan, X.G. Topological materials discovery by large-order symmetry indicators. *Sci. Adv.* **2019**, *5*, eaau8725. [CrossRef] [PubMed]
26. Xu, L.; Sevov, S.C. Heteroatomic deltahedral clusters of main-group elements: Synthesis and structure of the Zintl ions $[In_4Bi_5]^{3-}$, $[InBi_3]^{2-}$, and $[GaBi_3]^{2-}$. *Inorg. Chem.* **2000**, *39*, 5383–5389. [CrossRef]
27. Adam, M.; Hovestreydt, E.; Ruf, M.; Kaercher, J. Reaching a new highpoint with crystallography software -APEX3. *Acta Crystallogr. Sect. A Found. Adv.* **2015**, *71*, s194. [CrossRef]
28. Farrugia, L. WinGX suite for small-molecule single-crystal crystallography. *J. Appl. Crystallogr.* **1999**, *32*, 837–838. [CrossRef]
29. Sheldrick, G.M. Crystal structure refinement with SHELXL. *Acta Crystallogr. C* **2015**, *71*, 3–8. [CrossRef]
30. Momma, K.; Izumi, F. VESTA 3 for three-dimensional visualization of crystal, volumetric and morphology data. *J. Appl. Crystallogr.* **2011**, *44*, 1272–1276. [CrossRef]
31. Lacroix-Orio, L.; Tillard, M.; Belin, C. Synthesis, crystal and electronic structure of $Li_8Zn_2Ge_3$, a compound displaying an open layered anionic network. *Solid State Sci.* **2006**, *8*, 208–215. [CrossRef]
32. Stegmaier, S.; Fässler, T.F. Lithium-Stuffed Diamond Polytype Zn-*Tt* Structures (*Tt* = Sn, Ge): The Two Lithium-Zinc-Tetrelides $Li_3Zn_2Sn_4$ and Li_2ZnGe_3. *Inorg. Chem.* **2013**, *52*, 2809–2816. [CrossRef] [PubMed]
33. Mantina, M.; Valero, R.; Cramer, C.J.; Truhlar, D.G. *Atomic Radii of the Elements*; CRC Press: Boca Raton, FL, USA, 2013.
34. Yamada, T.; Yamane, H.; Nagai, H. A Thermoelectric Zintl Phase $Na_{2+x}Ga_{2+x}Sn_{4-x}$ with Disordered Na Atoms in Helical Tunnels. *Adv. Mater.* **2015**, *27*, 4708–4713. [CrossRef]
35. Kanno, M.; Yamada, T.; Yamane, H.; Nagai, H. Synthesis, Crystal Structure, and Thermoelectric Properties of $Na_{2+x}Al_{2+x}Sn_{4-x}$ (x = −0.38, −0.24). *Chem. Mater.* **2016**, *28*, 601–607. [CrossRef]